Giant unilamellar vesicles : an efficient membrane biophysical tool and its application in drug delivery studies

Lopez Mora, N.F.

Chapter III

The effect of crosslink density on hydrogel-assisted giant unilamellar vesicle growth

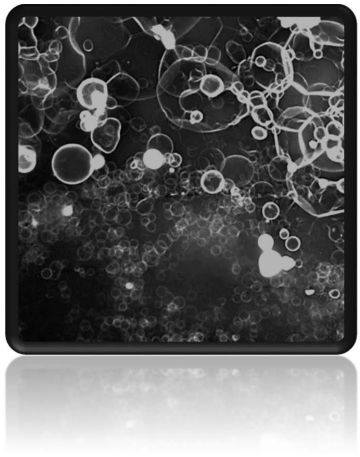

Manuscript in preparation: Nestor Lopez Mora, Yue Gao, M. Gertrude Gutierrez, Justin Peruzzi, Ivan Bakker, Ruud J.R.W. Peters, Bianka Siewert, Sylvestre Bonnet, Roxanne E. Kieltyka, Jan C. M. van Hest, Noah Malmstadt and Alexander Kros

Abstract.

Giant Unilamellar Vesicles (GUVs) are becoming popular membrane model systems for use in biophysical studies. The quality, size and yield of GUVs depend on the preparation method. In this study hydrogels consisting of dextran polymers crosslinked by poly(ethylene glycol) (DexPEG) were used as hydrophilic frameworks for the preparation of vesicle suspensions at physiological ionic strength conditions. A comparative study was performed using hydrogels with varied mechanical and morphological properties to evaluate their performance for GUV production. The efficiency of GUV production was quantified by flow cytometry with the size distribution being estimated by the Coulter Principle. We find that hydrogels of lower mechanical strength and increased swellability promote the production of GUVs, while their resulting size is determined by the surface roughness of the hydrogel film.

Introduction

The cellular membrane defines the boundary between the cytoplasm and the cell exterior regulating important intra- and intercellular processes in the biological milieu.[1] Therefore, the necessity of minimal cell models that allow *in vitro* studies, thereby simplifying these investigations, becomes highly relevant.[2] Giant Unilamellar Vesicles (GUVs) are exploited *in vitro* as a biomembrane model because of their membrane curvature and similarity in size to cells, being readily observable by optical microscopy.[3, 4] The GUV model has been used in the study of biomembrane properties,[5-8] membrane-protein[9-13] and membrane-peptide interactions,[14] channel formation in membranes[15, 16] or transmembrane transport of ions.[17, 18] Thus, the efficient formation of high quality GUVs under relevant physiological conditions is highly desirable.

The use of hydrogels as substrates for GUV growth is attractive due their potential to circumvent the disadvantages encountered in traditionally used methods such as natural swelling[19] and electroformation.[20] Covalent hydrogels are insoluble crosslinked polymer networks consisting of hydrophilic precursors that swell rapidly upon the addition of water creating a three dimensional network structure.[21] Most often, such networks have been applied in the areas of controlled drug delivery[22-24] and tissue engineering,[25, 26] but rarely in the growth of cell-sized vesicles (GUVs). Only recently, it has been shown that the use of hydrogel films enables the formation of GUVs at relevant physiological conditions. Horger et. al.[27] have proposed the use of physical gel substrates based on non-crosslinked agarose for the preparation of GUVs at near physiological conditions. The hydrogel produces GUVs successfully with several lipid compositions. However, traces of the agarose hydrogel substrate in the vesicle inner volume and the lipid membrane affect their mechanical properties. To tackle these drawbacks Lira *et al.*[28] used a thermal post-treatment of agarose-GUVs to release the encapsulated agarose and recover the GUV responses in electrodeformation studies. Alternatively films of hydrogels based on poly(vinyl alcohol)[29] and crosslinked polyacrylamide[27] have also been employed for the preparation of GUVs. While these polymers are not detected in the lipid bilayer of GUVs, they afford minimal control over the production and size.[30] We recently presented a facile method to form GUVs under physiological ionic strength conditions using a neutral, chemically crosslinked hydrogel substrate (DexPEG) consisting of a dextran polymer cross-linked by polyethylene glycol (PEG).[31] Maleimide-thiol

coupling chemistry was used to simultaneously crosslink the polymer chains and to anchor the forming gel to a glass surface. Chemically anchoring the hydrogel to the glass surface prevents its detachment during the rapid swelling of the DexPEG hydrogel film upon immersion of the glass slides in water. The use of the biocompatible DexPEG polymer that rapidly imbibes water from the dry state enables the formation of GUVs upon rehydration of a lipid film using physiologically relevant buffers.

Herein, we examine the effect of modulating hydrogel physicochemical properties on GUV production by controlling the crosslink density. We synthesised various DexPEG hydrogels by reacting a dextran polymer containing a controlled number of maleimide moieities and polyethyleneglycol (PEG) polymers with varied architecture, molecular weight and number of thiol functionalities (**Scheme 1** and **Table 1**). The production of GUVs on the various DexPEG hydrogel substrates was compared with respect to GUV size and yield by flow cytometry using the same lipid composition, ionic strength and growth times. The GUV formation process during hydrogel swelling was followed by imaging vesicle growth in time to better understand the effect of the various DexPEG substrates.

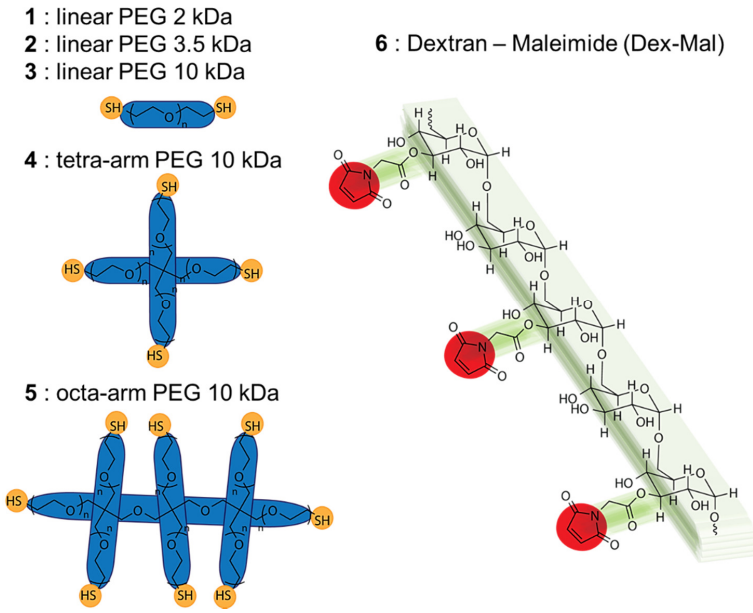

Scheme 1. Chemical structures of the precursors in the DexPEG hydrogel.

Table 1. Combinations of precursors for the formation of DexPEG hydrogels used in this study.

PEG crosslinker	Dex-Mal (**6**) DS=2	Dex-Mal (**6**) DS=4	Dex-Mal (**6**) DS=6	Dex-Mal (**6**) DS=9	Dex-Mal (**6**) DS=12
PEG (**1**)	✓	✓	✓	✓	✓
PEG (**2**)	✓	✓	✓	n.p.	✓
PEG (**3**)	n.p.	✓	n.p.	n.p.	n.p.
PEG (**4**)	✓	✓	✓	n.p.	✓
PEG (**5**)	✓	✓	✓	n.p.	✓

n.p. Not prepared

Results and Discussion

The degree of substitution (DS) and the architecture of the polymer crosslinker were systematically varied to modulate the physicochemical properties of the hydrogel materials (**Scheme 1**). Esterification of the dextran polymer with various equivalents of *N*-Maleoyl-*β*-alanine at room temperature resulted in functionalized polymers with a varying degree of substitution. The DS of the maleimide modified dextran (Dex-Mal), defined as the number of maleimide groups per 100 glucopyranose residues of dextran, was characterized by ^{1}H NMR. A proportional increase in the DS with the number of equivalents of *N*-Maleoyl-*β*-alanine added was observed up to DS=6. For DS>6, the addition of smaller quantities of *N*-Maleoyl-*β*-alanine resulted in greater changes in DS values (**Figure 7**, *Experimental Section*). Successful reaction of *N*-Maleoyl-*β*-alanine with the dextran polymer was confirmed by IR spectroscopy through the growth of the band 1700 (C=O), 1650 and 700 (vinyl) cm-1 increasing sharply with substitution degree (**Figure 8**, *Experimental Section*). In order to form hydrogels, thiolated linear (molecules **1**, **2** and **3**), tetra-arm or octa-arm PEGs (molecules **4** and **5**) were mixed to the various Dex-Mal polymers at a 1:1 molar ratio (maleimide:thiol) resulting in crosslinking of polymers via Michael addition. The polymer mixture (DexPEG) was drop-casted on thiolated glass slides as previously described.[31] The quality of the hydrogel film formed on the glass surface varied with DS by visual inspection. DexPEG polymers with a DS from 2 to 4 produced clear and homogeneous films on the glass surface regardless of the

architecture of the PEG crosslinker used, whereas higher DS dextran polymers resulted in inhomogeneous hydrogel films.

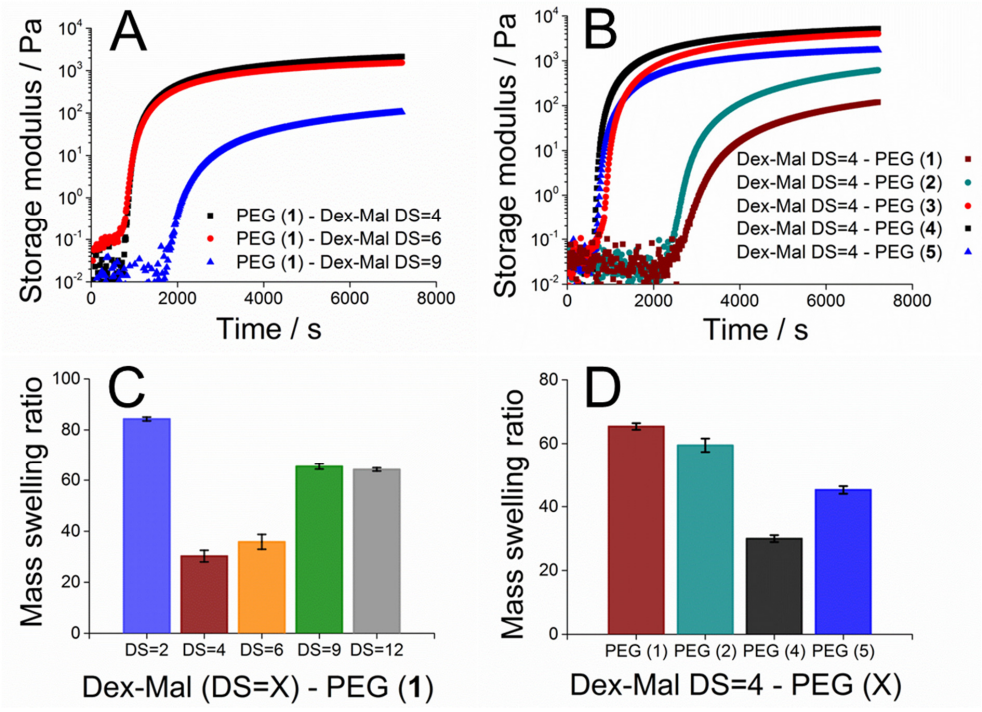

Figure 1. Mechanical and equilibrium swelling data of various DexPEG hydrogels with varied DS of the maleimide units in the dextran backbone and crosslinker (molecules **1**–**5**). *Top:* Oscillatory time sweeps for DexPEG hydrogels: **A**) **1** (1.2 wt %) and **6** (3.5 wt %) with DS = 4, 6 and 9. **B**) Molecules **1**–**5** and **6** with a DS = 4. *Bottom:* Equilibrium mass swelling ratio for DexPEG hydrogels with **C**) **1** and **6** DS = 2, 4, 6, 9 and 12. **D**) Molecules **1**– **5** and **6** (DS = 4).

Oscillatory rheology time sweeps were performed to provide insight into the gelation time and mechanical properties of the various DexPEG hydrogels. Their mechanical strength was examined as a function of the DS in Dextran (**6**) and the molecular weight, the number of thiols, and architecture of the crosslinker precursor (**1**, **2**, **3**, **4** and **5**). DexPEG combinations with higher DS in **6** produced weaker network structures with slower gelation rate (**Figure 1A**),

while higher molecular weight of the crosslinker precursor resulted in faster gelation and stronger networks (**Figure 1B**). Loose network structures were formed with linear based gels architecture (**1**, **2**) and interestingly, tetra-arm PEG (**4**) produced higher storage modulus than the octa-arm PEG (**5**) architecture which contains two times more thiol reactive groups. This phenomenon has been previously reported for hydrogel networks bearing substantial amounts of intramolecular loops or unreacted groups in the polymer network.[26]

The swelling properties of DexPEG hydrogels were examined to better understand the rehydration of the dried hydrogel films during the GUV formation. We studied the equilibrium mass swelling ratio of DexPEG hydrogels in glass vials excluding lipids. The equilibrium mass swelling ratio is defined as *Ws*/*Wd*, where *Ws* is the swollen weight of the gel after equilibration in buffer and *Wd* is the dry weight of the lyophilized gel. The swelling ratio decreases when the DS in Dex-Mal (**6**) increases, but for higher DS this trend is reversed (**Figure 1C**). This increase in the swelling ratio data revealed that those DexPEG combinations consist of a loose network structure. The opposite was observed with increasing the number of thiols in the PEG crosslinker, resulting in decreased swelling (**Figure 1D**). Consistent with mechanical measurements, the DexPEG hydrogel containing octa-arm PEG displayed a higher swelling ratio as compared to hydrogels crosslinked with tetra-arm PEG. This result is most likely due to the restricted accessibility of thiol groups on the octa-arm PEG to react efficiently with maleimides on the dextran polymer (Dex-Mal, molecule **6 Scheme 1**). Thus, the presence of more reactive groups on the same polymer chain increase the probability of reacting on the same polymer chain, producing more defective, looser and sweallable polymeric networks.

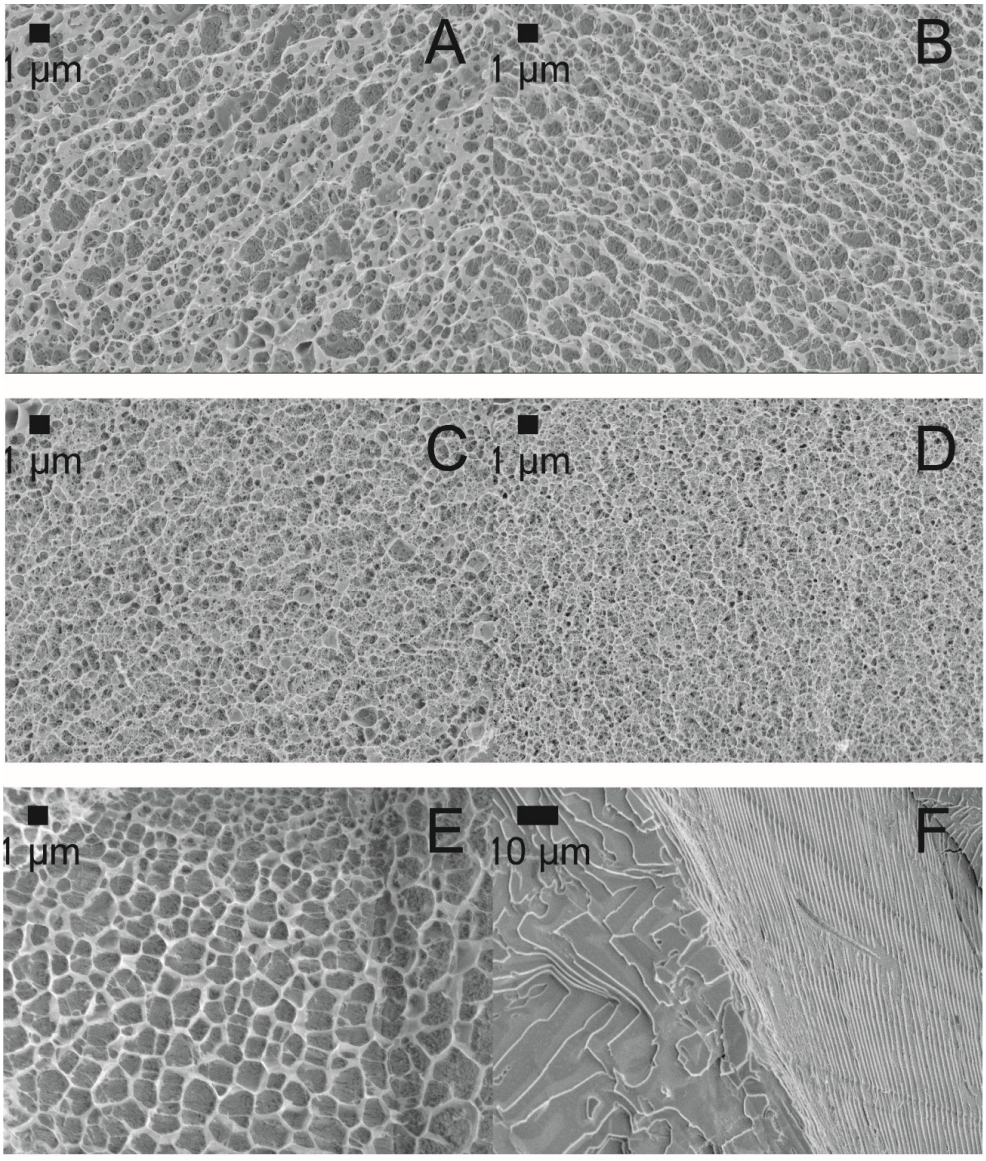

Figure 2. Cryo-SEM of DexPEG hydrogels with different DS and PEG crosslinker. **A**) **6** DS=4 and crosslinker **1**; **B**) **6** DS=4 and crosslinker **2**; **C**) **6** DS=4 and crosslinker **4**; **D**) **6** DS=4 and crosslinker **5**, **E**) **6** DS=6 and crosslinker **2**, **F**) **6** DS=12 and crosslinker **2**. The effect of the crosslinker in the morphology of hydrogels can be observed in Figures 2A and 2B for DexPEG hydrogel containing linear PEG (**1, 2**), Figure 2C for DexPEG hydrogel containing tetra-arm PEG (**4**) and Figure 2D for DexPEG hydrogel containing octa-arm PEG (**5**).

Next, we examined the morphology of selected DexPEG hydrogels in the swollen state by cryo-scanning electron microscopy (cryo-SEM), see **Figure 2**. We observed that hydrogels composed of **6** with a DS>6 lacked the ability to form a three dimensional network structure (i.e. **Figure 2F**). In contrast, hydrogels with a DS<6 produced a continuous honeycomb-like network structure in the swollen state, but with different pore size. For example, the DexPEG hydrogel with DS=6 (**Figure 2E**) forms a porous network morphology with pore sizes greater (~1 μm) whereas a hydrogel with DS=4 (**Figure 2B**) displays pore sizes around 200 nm in size. This finding is in contrast to photocrosslinked dextran-methacrylate hydrogels containing the same dextran backbone, where the pore size decreased when the degree of substitution increased.[32] A possible explanation may be due to the decreased solubility of Dex-Mal (**6**) in water when the degree of substitution is increased, while the solubility of methacrylate functionalized dextran is not significantly affected by the DS. Additionally, increasing the number of thiol groups in the PEG crosslinker yielded DexPEG hydrogels with a highly porous honeycomb-like structure.

We found previously that DexPEG hydrogels with a decreased crosslink density present the ability to growth GUVs with larger mean diameter.[31] The morphology of those hydrogels was also examined by cryo-SEM as a function of the maleimide/thiol ratio (**Figure 9**, *Experimental Section*). Overall, these results show that decreasing the PEG crosslinker concentration leads to formation of an inhomogeneous network structure due to the formation of fewer crosslinks. These observations are in good agreement with the mechanical data (**Figure 10**, *Experimental Section*) that point to the formation of a weak and loose network structure consistent with the crosslink density.

The correlation between hydrogel crosslink density and its effect on GUV yield was quantified by fluorescence-activated cell sorting (FACS) experiments. Stock solutions of the lipid mixtures POPC : Cholesterol (80 : 20 mol%) and POPC : Cholesterol : PEG2000-PE (75 : 20 : 5 mol%) were deposited on the DexPEG hydrogel coated microscope slides with varied DS and crosslinkers. Both lipid compositions also contained 0.7 % mol of 1,2-dioleoyl-*sn*-glycero-3-phosphoethanolamine-*N*-(7-nitro-2-1,3-benzoxadiazol-4-yl) (ammonium salt) (DOPE-NBD) to allow fluorescence detection of the formed GUVs. Subsequently, the solvent was evaporated under a gentle stream of nitrogen and in a vacuum oven overnight. Finally, the lipid-coated hydrogel films were hydrated in phosphate-buffered saline (PBS) and the resulting free-floating GUVs were collected and characterized by FACS. PEGylated and non-PEGylated

GUVs were formed on all hydrogels and detected in both fluorescence and side scattering channels, producing typical populations of GUVs (**Figures 11** and **12**, Experimental Section). The use of PEGylated lipids in the lipid composition of GUVs decreased the aggregation of GUVs, resulting in an increased frequency of single events (i.e. a more precise counting of single GUVs) for all DexPEG combinations (**Figure 3**). Firstly, increasing the DS in Dex-Mal resulted in a higher GUV yield (**Figure 3A**). These observations were in good agreement with the swelling ratio studies confirming that this is the main parameter in GUV formation. In contrast, increasing the number of thiol groups of PEG crosslinkers decreased the yield of GUVs (**Figure 3B**). Only hydrogels synthesized with the octa-arm PEG (**5**) did not follow this trend also in line with swelling data. The effect of the degree of substitution and crosslinker density on GUVs production is in good agreement with the oscillatory rheology, equilibrium mass swelling ratio, and SEM imaging of the various DexPEG substrates. Moreover, these results inidicate that the main driving force for efficient GUV production is the high swellability of the dextran hydrogel network during the rehydration of the lipid-coated hydrogel films.

The size distribution of the produced GUVs was estimated using the Coulter Principle in a Quanta SC FACS instrument based on electrical impedance.[33, 34] The Electric Volume (*EV*) parameter is proportional to the electrical impedance and does not depend on the laser wavelength, geometry or refractive index of the sample, overcoming limitations of forward and side scattering monotonic measurements for the determination of particle size by flow cytometry.[35] We transformed the *EV* parameter measured to GUV diameter (μm) (See **equation 1** and **2** in *Experimental Section*). Validation of this method was made with microsphere standards with nominal sizes of 10 μm and 20 μm (**Figure 13**, *Experimental Section*). These measurements yielded a size distribution profile for a large set of PEGylated GUVs. The advantage of this method is the possibility to count large populations of GUVs, as compared to microscopy-based methods which can only consider smaller population sizes due to the small focal volume.

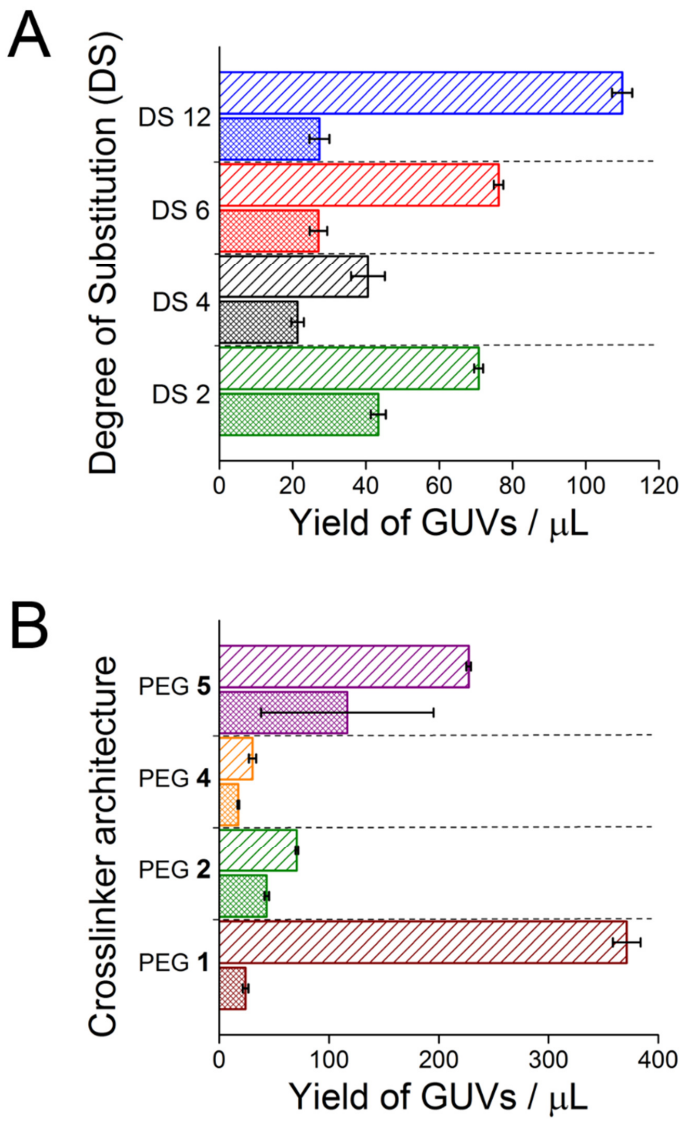

Figure 3. Yield of fluorescently labelled GUVs produced on the various DexPEG substrates as determined by FACS. Cross-hatched bars represent GUVs with the lipid composition POPC : Cholesterol (80 : 20 mol%) and line patterned bars represent PEGylated GUVs with the lipid composition POPC : Cholesterol : PEG2000-PE (75 : 20 : 5 mol%). **A**) Effect of the DS on the production of GUVs for DexPEG hydrogel films with linear crosslinker **2** and **6** DS from 2 – 12. **B**) Effect of the functionality of the PEG crosslinker on the production of GUVs for DexPEG hydrogel films with **6** DS=2 and linear PEG (**1**), linear PEG (**2**), tetra-arm PEG (**4**) and octa-arm PEG (**5**) crosslinkers.

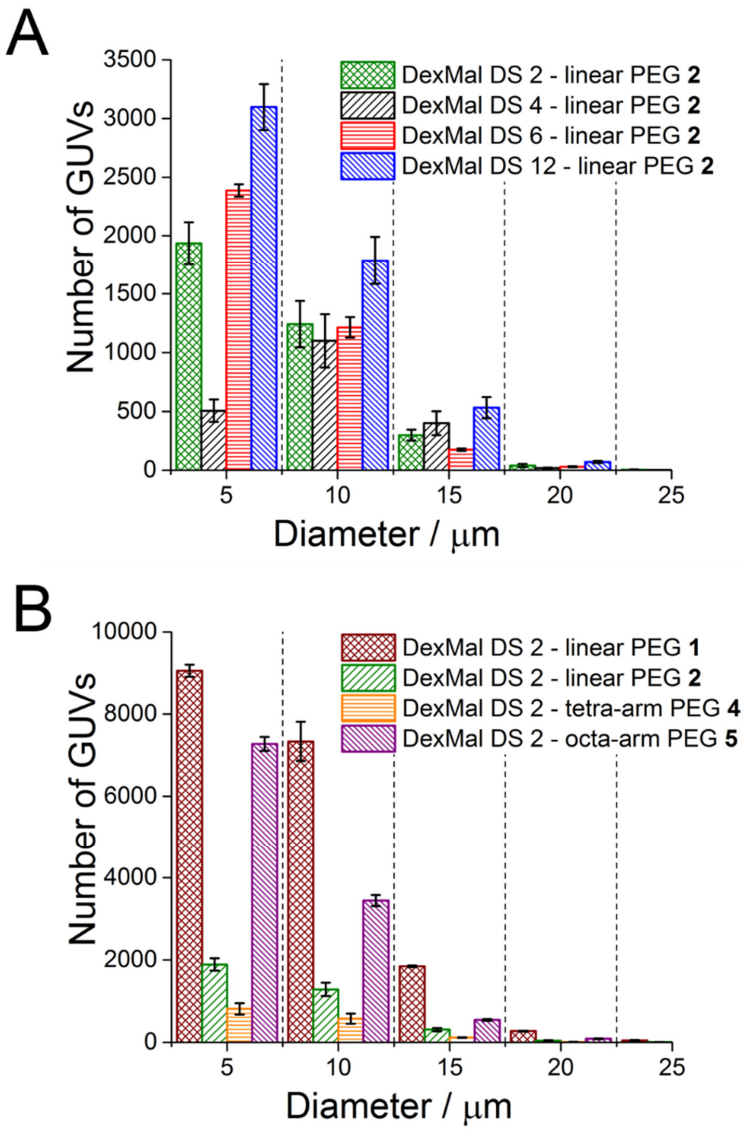

Figure 4. Determination of the size distribution by the Coulter principle for GUV populations with the lipid composition POPC:Cholesterol:PEG2000-PE (75 : 20 : 5 mol%) produced on various DexPEG substrates. **A**) Effect of the DS on the size of GUVs for DexPEG hydrogel films with linear crosslinker **2** and **6** with DS from 2–12. **B**) Effect of the functionality of the PEG crosslinker on the size of GUVs for DexPEG hydrogel films with **6** DS=2 and linear PEG (**1**), linear PEG (**2**), tetra-arm PEG (**4**) and octa-arm PEG (**5**) crosslinkers.

In **Figure 4**, the effect of the DS and the crosslinker functionality of the hydrogels on the GUV size distribution are presented. All tested DexPEG hydrogel substrates, independent of the DS or crosslinker functionality, produced GUVs populations with sizes ranging between 5 µm and 20 µm in diameter. DexPEG hydrogels designed with multi-arm PEG crosslinkers **4** and **5** produced GUVs with a similar size distribution as compared to linear PEG crosslinker **1** and **2** based hydrogels, but with lower yields. These size distributions are in line with those previously reported by optical microscopy using a lipid composition of POPC : Cholesterol (80 : 20 mol%) on DexPEG substrates with equimolar ratio of precursors (diameter = 10 ± 5 µm, N = 55 GUVs).[31] Moreover, we previously found that by decreasing the crosslink density by reducing the molar ratio of PEG (**1**) crosslinker respect to Dex-Mal (**6** DS=4) the GUVs size distribution could be tuned. In this work, we further explore the potential to tune GUV size by increasing the crosslink density through the use of multi-arm PEG crosslinkers **4** and **5**. No significant differences in the GUVs size distribution were observed, however lower yields due to the decreased swelling of these networks were observed (**Figure 4B**). Collectively, these data together with oscillatory rheology and cryo-SEM imaging of those hydrogels (*vide supra*) indicate that the formation of inhomogeneous and loose networks by decreasing the crosslink density leads to wider and larger size distributions of GUVs, while the formation of homogeneous and compact networks with small pore sizes does not affect significantly the size distribution the GUVs.

The GUV formation and growth from DexPEG hydrogels was studied by differential interference contrast (DIC) microscopy. Lipids (POPC : Cholesterol, 80 : 20 mol%) were spread on DexPEG hydrogels composed of linear PEG (**1**) and tetra-arm PEG (**4**) crosslinkers and observed before and during swelling. The hydrogel was swollen with 200 mM sucrose in PBS (pH 7.4) and images were taken every second for 10 minutes. The initial GUV diameter was a few microns and became larger due to coalescence from crowding. Most likely, the GUVs take on the size of the pores of the honeycomb network of DexPEG upon exposure to the buffer. These GUV coalescence events are quantified as a function of time in **Figure 5A**. Upon GUV coalescence, the average size of GUVs increases while the number of GUVs decreases. Variation in the initial GUV sizes was observed as a function of the varying surface roughness within the hydrogel of the DexPEG with linear PEG (**1**) and tetra-arm PEG (**4**). Meticulous inspection of hybrid lipid/DexPEG hydrogel film showed rougher surfaces and smoother surfaces consistent with the quality of the drop-casted gel. On rougher surfaces (**Figure 5B**) GUVs coalesced less and maintained a smaller size (~5 µm diameter), while in

smoother surfaces (**Figure 5C**), the formed GUVs were larger (~14 μm diameter). Therefore thickness and roughness of the DexPEG hydrogel film should be considered for controlling polydispersity in the final size distribution of GUVs.

Overall, the physical data obtained by oscillatory rheology, equilibrium swelling and cryo-SEM show that the number of thiols and polymer architecture strongly affect the effective crosslinking density of hydrogel network formed via maleimide-thiol addition. Examining the physicochemical properties of the various combinations of the DexPEG hydrogels revealed that a lower mechanical strength and an increased swelling ratio of the network favour GUV growth, whereas an increased crosslink density negatively impacts the lipid self-assembly process. GUVs swell from the surface of the hydrogel matrix (DexPEG) as depicted in **Figure 6**. Here, the growth of fluorescent labelled GUVs is shown using a confocal microscopy imaging reconstruction. The orthogonal reconstruction of the confocal image allows the imaging of the budding of vesicles during the first minutes of lipid hydration on the hydrogel scaffold.

Finally, we investigated the interaction of lipids with a dry DexPEG film. The gel to liquid-crystalline phase transition of DOPC lipids in the presence and absence of DexPEG film was determined by differential scanning calorimetry (DSC). A single sharp endothermic transition (T_m) was found for pure DOPC at -6 °C, meaning that the water/lipid ratio was ~3.[36] The T_m for DOPC on a DexPEG film shifted to -18 °C and was broadened (**Figure 14A**, *Experimental Section*), indicative of lipid-DexPEG interaction. For comparison we also determined the T_m of DOPC in the presence of only PEG gel (2 wt% of tetra-arm PEG (**4**), crosslinked with 0.05 vol% H_2O_2, *Experimental Section*). Surprisingly, the T_m of DOPC was now fully depressed (**Figure 14B**, *Experimental Section*). This finding shows that DOPC interacts more strongly with PEG as compared to dextran. Moreover, the growth of GUVs on films of PEG (**4**) gel was not observed. Therefore lipid-hydrogel interactions should be considered when designing new hydrogels for GUV formation and studies understanding these interactions are required.

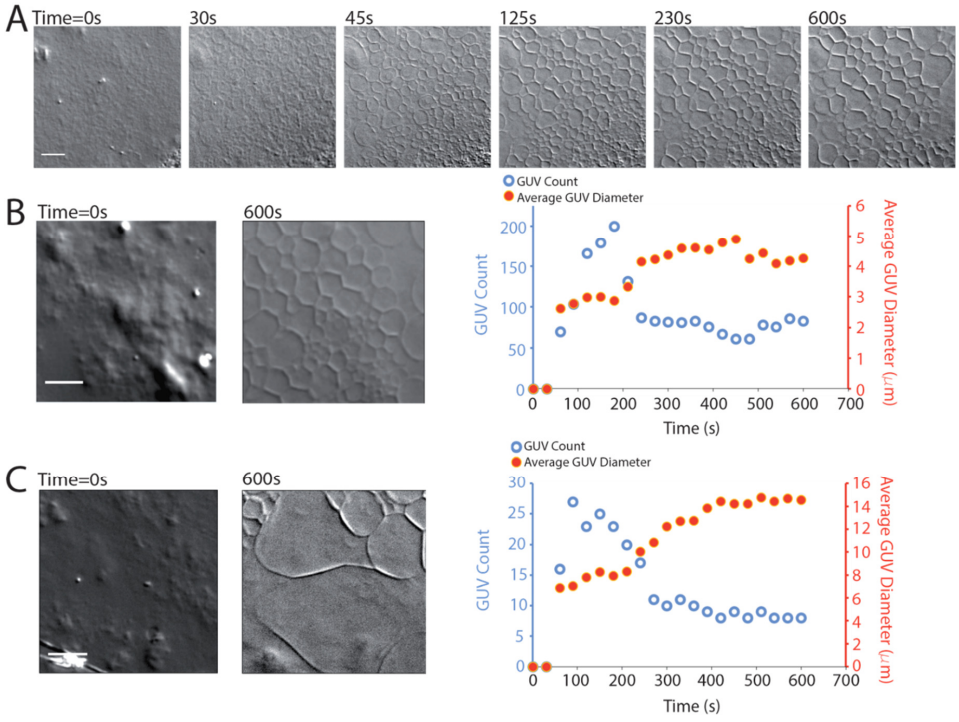

Figure 5. GUV swelling observed on the DexPEG surface. **A**) DIC time lapse series of micrographs of POPC : Cholesterol (80 : 20 mol%) on DexPEG hydrogel with DS=2 and tetra-arm PEG (**4**) crosslinker. The scale bars are 10 μm. The first image shows dried lipid film on top of the hydrogel. The subsequent images are indicated according to time of swelling. GUVs form off of the DexPEG hydrogel network and coalesce to form larger GUVs. **B**) Left micrographs show areas of rough DexPEG with lipid before hydration (Time=0s) and after hydration (600s). The right plot shows how GUV number and average size changes with time. **C**) Micrographs are examples of areas of smooth DexPEG with lipid and associated kinetics of swelling plot is on the right. As coalescence occurs, GUV size increases and count decreases. Smooth DexPEG areas form larger GUVs as compared with rougher areas.

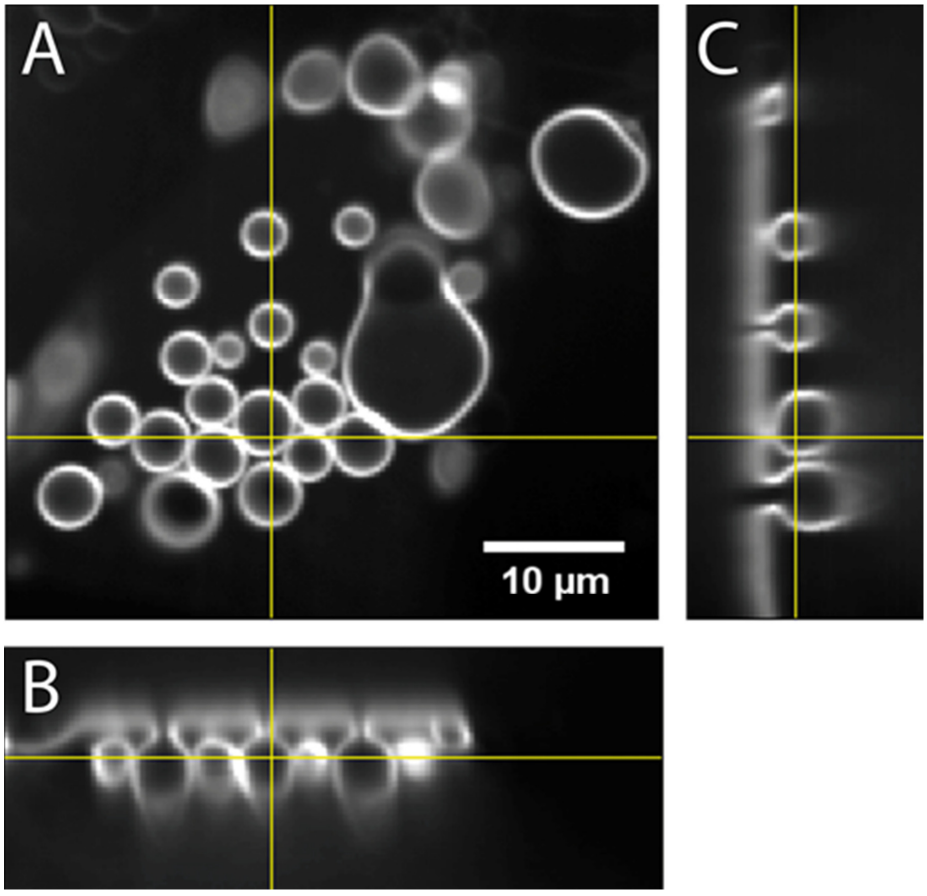

Figure 6. Confocal images GUVs formed from a DexPEG surface. **A**) A single confocal slice of an image stack of GUVs swollen on DexPEG. Lipid composition is POPC : Cholesterol (80 : 20 mol%) fluorescently labelled with ATTO-488-DPPE (0.4 mol%). The yellow lines indicate the orthogonal slices in B and C. **B**) Horizontal orthogonal slice of GUVs in A reconstructed from confocal image stack. **C**) Vertical orthogonal slice of GUVs in A. B and C show GUVs that are not yet fully formed closed spheres. Rather, they are still attached by budding necks to the surface of the lipid film.

Conclusion

In conclusion, we designed a very facile and efficient method for GUV preparation. The effect of increased crosslinking on the dextran hydrogel by poly(ethylene glycol) on the yield, size distribution and formation of GUVs revealed that the physicochemical properties of DexPEG hydrogels strongly influence the production of GUVs in PBS. The most optimal hydrogel scaffolds for GUV growth exhibit the highest swelling capacities. Furthermore, we observed that the final size distribution of the GUVs is not affected by the honeycomb architecture of the DexPEG substrate but rather by the homogeneity of the network and surface roughness of the film. We envisage that controlling the roughness of the DexPEG film might provide a way to produce monodisperse GUVs populations. Finally, hybrid lipid/DexPEG films facilitate the budding and coalescence of vesicles to produce high yields of GUVs under high ionic strength. The efficient formation of GUVs at physiological salt concentrations has the potential to increase the applicability of GUVs as a biophysical model in the study of membrane interactions at similar conditions than those required in *in vivo* systems.

Experimental Section

Materials and methods

1-palmitoyl-2-oleoyl-*sn*-glycero-3-phosphocholine (POPC), 1,2-dioleoyl-*sn*-glycero-3-phosphoethanolamine-*N*-[methoxy(polyethylene glycol)-2000] (ammonium salt) (PEG2000-PE) and 1,2-dioleoyl-*sn*-glycero-3-phosphoethanolamine-*N*-(7-nitro-2-1,3-benzoxadiazol-4-yl) (ammonium salt) (18:1 NBD-PE) were purchased from Avanti Polar Lipids. Dextran from Leuconostoc (M_n = 70 000, dried in vacuum oven for several days before use), Cholesterol (CH), *β*-Alanine, 4-(dimethylamino) pyridine (DMAP), Magnesium Sulfate ($MgSO_4$), 3400 Da poly (ethylene glycol) dithiol, *N*,*N*'-Diisopropylcarbodiimide (DIC), Acetic Acid, Ethyl Acetate, Toluene, Dimethyl Sulfoxide (DMSO) and 2-propanol were purchased from Sigma-Aldrich. Maleic Anhydride and *p*-Toluene Sulfonic Acid Monohydrate (PTSA) were purchased from Fluka. 2000 Da poly (ethylene glycol) dithiol was purchased from Iris Technologies GmbH. 4 arms poly (ethylene glycol) thiol (pentaerythritol core) and 8 arms poly (ethylene glycol) thiol (tripentaerythritol core) were purchased from JenKem Technology, USA. NIST Traceable Latex Particles Standards nominal sizes 10 µm and 20 µm were purchased from Beckman Coulter. The salt of pyridinium 4-(Dimethylamino) pyridinium 4-toluenesulfonate (DPTS) was prepared from DMAP and PTSA in equimolar quantities.[37]

*Synthesis and characterization of N-Maleoyl-β-alanine and Dex-Mal (**6**) with different degree of substitution.*

N-Maleoyl-*β*-alanine was prepared in a large scale synthesis following the previously reported procedure for obtaining maleimido alkanoic acids.[38] Maleic anhydride (9.95 g) and *β*-Alanine (9.18 g) were added to 75 mL acetic acid. The mixture was refluxed at 170 °C for 90 minutes. Then the solution was cooled to room temperature. The acetic acid was evaporated in vacuum. The residual acetic acid was removed by forming an azeotrope with toluene and evaporation under vacuum. The crude was extracted three times in ethyl acetate and the organic layer was dried with $MgSO_4$. The crude was recrystallized in ethyl acetate at 4 °C overnight.

The compound was sublimed using a cold finger to increase the purity. The final yield is 31.6 %. The compound was characterized with ^{1}H-NMR (400MHz, $CDCl_3$): δ = 6.7 (s, -C**H**=C**H**-), δ = 3.8 (HOOC-C**H**$_2$-CH$_2$), δ =2.7 (-CH$_2$-C**H**$_2$-N).

Dex-Mal (**6**) was synthesized by DIC mediated esterification of the hydroxyl groups of dextran with *N*-Maleoyl-*β*-alanine. For instance to obtain a substitution degree of 4, Dextran (0.62 g), *N*-Maleoyl-*β*-alanine (0.42 g) and DPTS (0.15 g) were dissolved in anhydrous DMSO (25 mL). The mixture was stirred at room temperature for two hours, followed by the addition of DIC (0.48 mL). After overnight stirring (19 hours) at room temperature, the formed *N*, *N*'-dialkylurea was removed by filtration and the crude product was obtained by precipitation in cold isopropanol. The precipitate was dissolved in water and extensively dialyzed against Milli-Q water for two days and subsequently lyophilized. ^{1}H NMR (400 MHz, D_2O): δ 3.3-4.0 (m, dextran glucopyranosyl ring protons), 4.9 (s, dextran anomeric proton), 6.8 (s, maleimide). ^{13}C NMR (400MHz, D_2O): δ=134.5, 97.7, 73.4, 71.4, 69.5, 65.5.

The degree of substitution (DS) of Dex-Mal is defined as the number of maleimide groups per 100 glucopyranose residues of dextran, which was calculated from the ^{1}H NMR spectra based on the protons of maleimide (δ 6.8) and the anomeric proton (δ 4.9). The DS of Dex-Mal was controlled by the molar ratio between Dextran and N-Maleoyl-β-alanine as it is showed in the **Figure 7**. The incorporation of *N*-Maleoyl-*β*-alanine in the Dextran backbone was confirmed by the presence of an ester FT-IR band at 1700 cm^{-1} (**Figure 8**). This band increases with the increase in the degree of substitution on the Dextran, while the broad hydroxyl group band between 3000 - 3700 cm^{-1} does not show a significant decrease, indicating the presence of hydroxyl free groups.

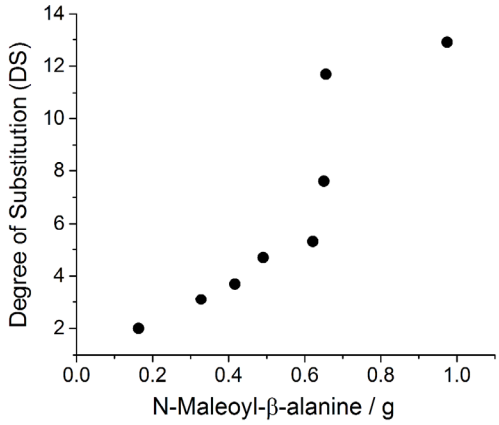

Figure 7. Degree of substitution (DS) as a function of the mass of *N*-Maleoyl-*β*-alanine added in the reaction to produce Dex-Mal (**6**). The degree of substitution (DS) of the product **6** is determined from the ^{1}H NMR.

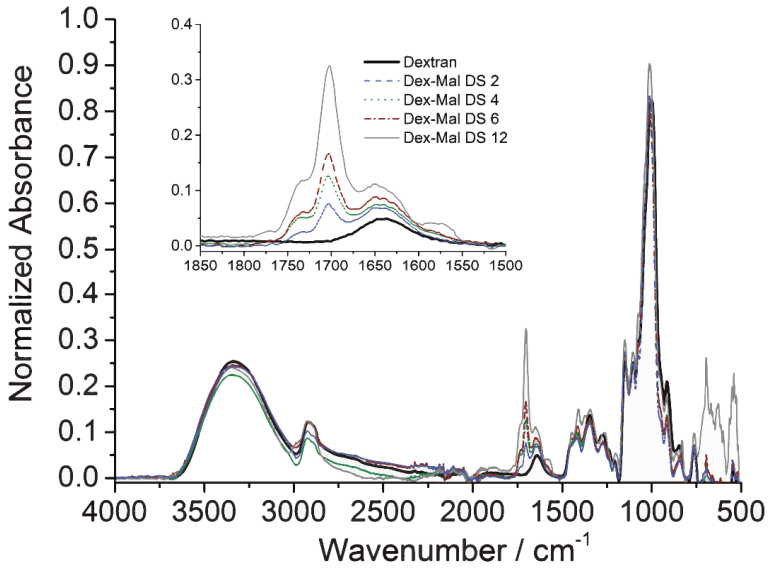

Figure 8. FT-IR spectra of Dextran and Dex-Mal (**6**) with degree of substitution (DS) 2, 4, 6, 12. The inset image shows the increase of the ester band (1700 cm^{-1}) corresponding to the bond between Dextran and *N*-Maleoyl-*β*-alanine.

DexPEG and PEG Hydrogel substrates preparation

DexPEG coated glass substrates. Dex-Mal (2 wt% solution, DS = 2, 4, 6 and 12) was crosslinked using **1**, **2**, **4** and **5** in equimolar ratios at room temperature to form several DexPEG hydrogels. For instance, Dex-Mal (**6**, DS= 4, 60 mg) was dissolved in water (2.5 g) and 11.11 mg of **1** (2000 Da) in water (0.5 g) were reacted to provide a DexPEG hydrogel solution. The mixture was shaken in a vortex for 1 minute and immediately used for the preparation of glass substrates. DexPEG solution (600 µL) was drop casted onto previously thiol functionalized microscope glass slides. A homogenous polymeric film was formed after evaporating water during 30 – 45 minutes at 40 °C. The DexPEG coated microscope slides were stored for further use.

PEG hydrogel coated glass substrates. Commercial 4-thiol armed PEG was crosslinked with hydrogen peroxide (H_2O_2) by forming disulfide tetramers. 4 armed- poly (ethylene glycol) thiol (pentaerythritol core) (**4**, 2 wt% solution) was dissolved in 100 µL water and mixed with 10 µL H_2O_2 (50 wt% in water). The mixture was shaken in a vortex for 1 minute and immediately used for the substrate preparation. Drop casting of the solution on thiol functionalized microscope slides resulted in the formation of an inhomogeneous hydrogel film after 5 minutes. The PEG coated microscope slides were stored for further use.

Formation of GUVs

Giant Unilamellar Vesicles (GUVs) were grown in various Dex-PEG hydrogel coated microscope glass slide substrates. A lipid solution (10 µL) with the lipid composition POPC and Cholesterol (80:20 molar ratio, 14 mM) and DOPE-NBD (0.7 mol%) or POPC / Cholesterol / PEG 2000 - PE (75 : 20 : 5 molar ratio, 14 mM) and DOPE-NBD (0.7 mol%) was deposited on a hydrogel coated glass slide, then the lipid solution was dried by evaporating the chloroform under a gentle stream of nitrogen and placed in a vacuum oven overnight. A liquid chamber was made by placing a 15 mm (OD) glass O-Ring on top of the hydrogel, which was sealed with high vacuum silicon grease. The lipid film was hydrated by adding 400 µL of PBS and the GUVs were growth overnight at room temperature.

Confocal and DIC Imaging.

Spinning-disc confocal microscopy was performed on a TI-Eclipse inverted microscope (Nikon, Japan) equipped with a 16-bit Cascade II 512 EMCCD camera (Photometrics, USA) and a CSUX confocal head (Yokogawa, Japan). Illumination was provided by a 50 mW solid-state laser at 561 nm (Coherent Inc., Germany) and the objective used was a 60× NA1.43 Plan-Apo Nikon oil-immersion objective. DIC imaging was performed on an Axio Observer (Zeiss, Germany) equipped with a Hamamatsu CMOS camera (Hamamatsu, Japan). Illumination was provided by a halogen lamp 12V 100W using a differential interference contrast prism with polarizer (Zeiss, Germany) and the objective used was a 20x NA0.8 Plan-Apo Zeiss objective.

Cryo-Scanning Electron Microscopy (cryo-SEM).

The morphologies of the hydrogels in the swollen states were observed in a JEOL 6330 Cryo Field Emission Scanning Electron Microscope from the General Instrumentation Facility at Radboud University (Nijmegen, The Netherlands). 5 μL of Dex-PEG hydrogel was taken and injected into a hollow cylindrical sample holder and immediately flash frozen in liquid nitrogen. The sample was then inserted in the cold-stage of the SEM cryo-preparation chamber and cleaved to make a horizontal fracture plane. The water was sublimated during 15 minutes and the fracture plane was coated with a thin gold-palladium layer and subsequently the sample is transferred into the SEM chamber, where it remained frozen during the imaging.

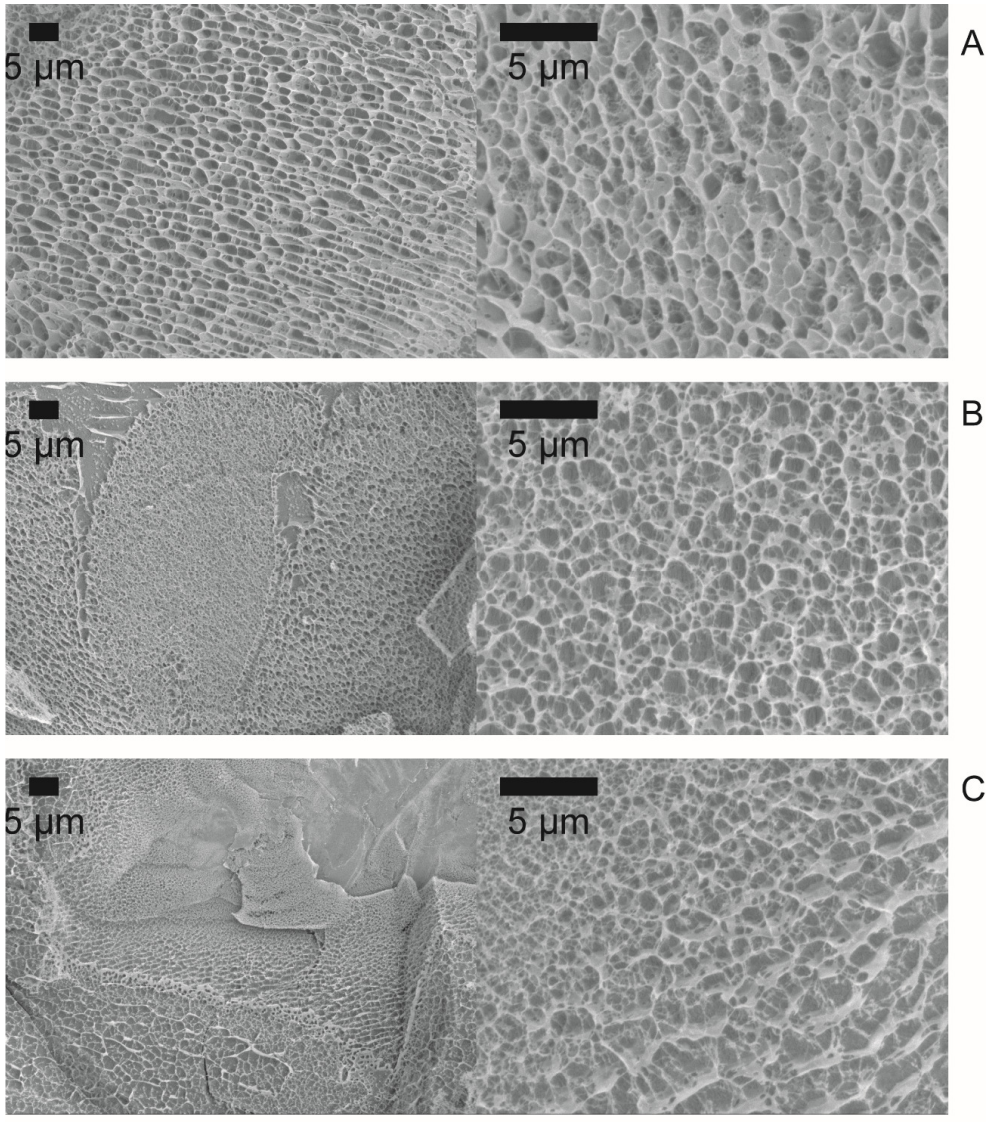

Figure 9. Cryo-SEM of DexPEG hydrogels with different molar ratio between precursors. **A**) Dex-Mal (DS 4) – PEG (**1**) crosslinker (1:1 molar ratio). **B**) Dex-Mal (DS 4) – PEG (**1**) crosslinker (1:0.75 molar ratio). **C**) Dex-Mal (DS 4) – PEG (**1**) crosslinker (1:0.5 molar ratio).

Oscillatory Rheology.

Oscillatory time sweeps were performed on a Hybrid Rheometer (DHR-2) from TA Instruments using a plate – plate geometry. The precursors Dex-Mal (**6**) with various DS and thiolated PEG solutions (molecules **1** – **5**) were loaded on the lower plate and the upper plate (25 mm diameter) was immediately lowered to a gap distance of 0.5 mm for all experiments. Oscillatory time sweeps were performed on the various forming hydrogel materials following the storage (G') and loss (G") moduli with respect to time at 1% strain and 0.1 – 100 rad/s angular frequency.

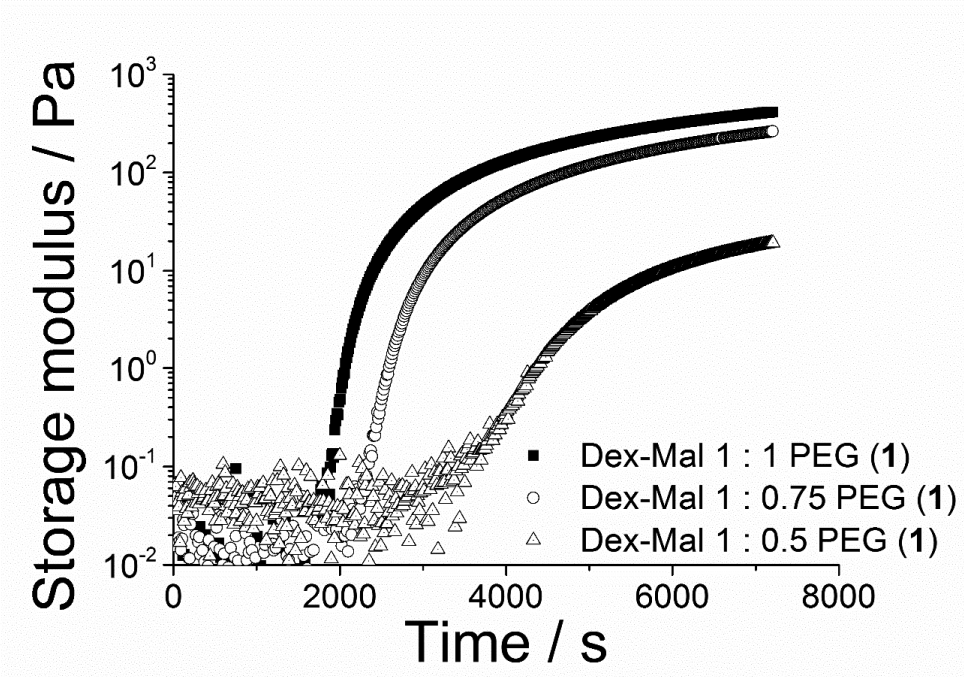

Figure 10. Mechanical characterization of DexPEG hydrogels with increasing PEG cross-linker using oscillatory rheology time sweeps. The trace in squares represents 1:1 molar ratio Dex-Mal (DS 4) – PEG (**1**). The trace in circles represents 1:0.75 molar ratio Dex-Mal (DS 4) – PEG (**1**). The trace in triangles represents 1:0.5 molar ratio Dex-Mal (DS 4) – PEG (**1**).

Flow Cytometry.

A Beckman Coulter Quanta instrument was used to analyze the yield and the size distribution of several GUV batches. In contrast to common fluorescence flow cytometers, which only depend on optical parameters, i.e. light scattering and fluorescence, the employed Beckman Coulter system additionally utilizes the electrical impedance, also known as Coulter Principle.[33, 39] Briefly, particles pass through the orifice of a saline-filled cell. A constant (DC) current is applied across this aperture with an electrical circuit. Whenever the nonconductive GUVs pass through this orifice a voltage pulse will be generated.[35] The amplitude thereof is theoretically proportional to the volume of the particles, and expressed as electric volume (*EV*). Based on the principle an accurate size measurement can be guaranteed, as the *EV* is in contrast to the forward scatter (*FSC*) monotonic.[35] In addition and simultaneously, each particle is irradiated by a 488 nm laser beam, leading to the possibility of detecting the side scatter (*SSC*), and therewith the density of the investigated particles, as well as light emission, thus fluorescence (available filters: 525 BP (*FL1*), 575 BP (*FL2*), 670 LP (*FL3*)).

Labelling of the lipid membrane of GUVs with DOPE-NBD ($\lambda_{max,\ abs}$ = 460 nm, $\lambda_{max,\ em}$ = 535 nm) allowed a clear distinction between sample and background or noise signals. A suspension of freshly prepared GUVs (500 µL) was gently mixed, transferred to a 24 well plate and placed in the auto sampler of the Beckman Coulter Quanta instrument. Before injecting the suspension (50 µL), the 24 well plate was orbitally shaken to avoid biases due to the settlement of GUVs and prevent the damage of the GUVs by harsh suspending through a syringe. The *EV*, *SSC* and *FL-1* signals of each GUV suspension were measured as a technical triplicate (see representative counter maps in **Figures 11** and **12**). As detection limit $1x10^5$ events was set. The raw data was exported as listmode files and processed with FlowJo. Only GUVs with a diameter >4 µm were considered in our analysis and all events showing a fluorescence signal were gated and defined as GUV population. The electronic volume values (*EV)* were exported to excel, transformed via **Eq. 1** into the electronic radius (*Er*), and thereafter standardized over **Eq. 2** utilizing fluorescent labeled standard beads (NIST traceable latex particle, indicated as STD in Eq. 2 with a nominal diameter of 10 µm. The ratio ($10\ \mu m/\mathrm{ER_{STD}}$) between the known diameter (10 µm) and the measured *Er* for the standard

(ER_{STD}) was used to transform the non-specified electronic volume of GUVs to the diameter in µm.

$$Er = \sqrt[3]{\frac{3}{4\pi}EV} \qquad \textbf{(Eq. 1)}$$

$$d_{GUV} = \frac{Er_{GUV}}{Er_{STD}} \cdot d_{STD} \qquad \textbf{(Eq. 2)}$$

The scale was verified with standard particles of 20 µm (see **Figure 13**), and the accuracy tested. The size of all the measured GUVs was categorized into five different groups for clarity, and the yield was expressed as GUVs per µL.

Access to FlowJo was kindly provided by Sander van Kasteren from the bio-organic synthesis group, Leiden University.

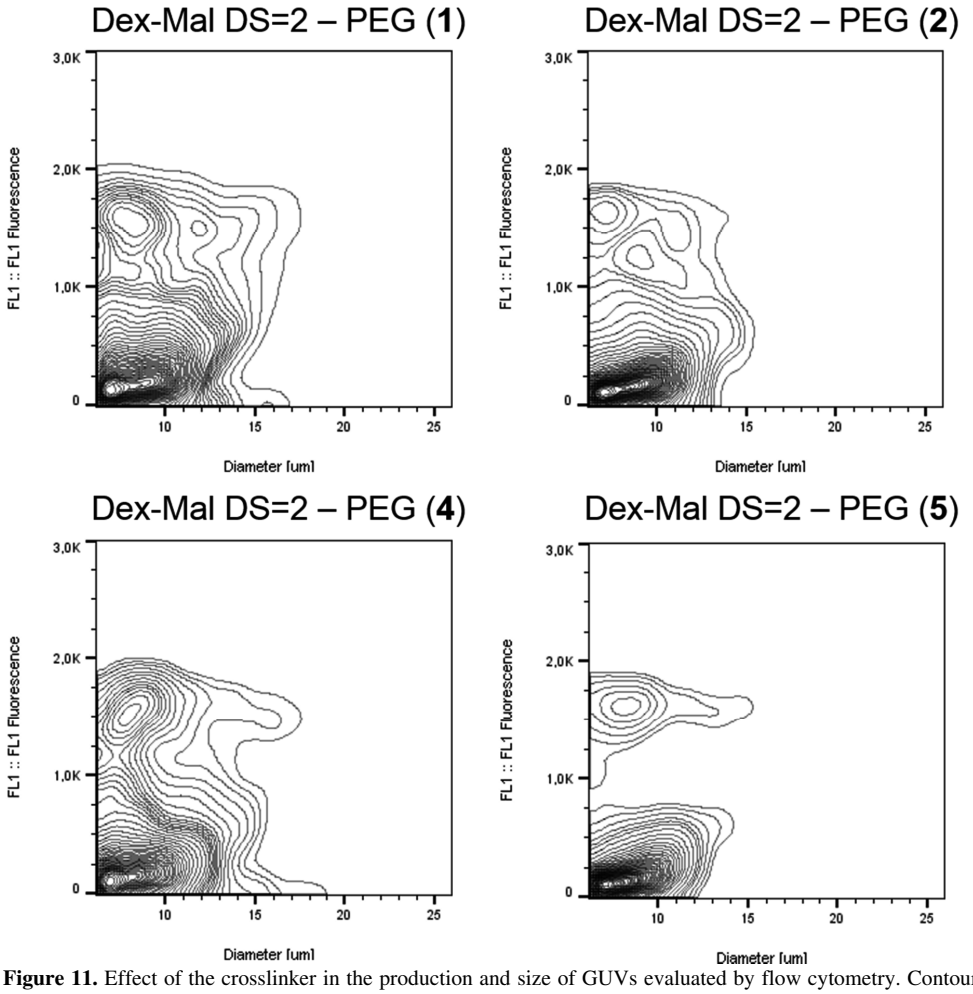

Figure 11. Effect of the crosslinker in the production and size of GUVs evaluated by flow cytometry. Contour maps of the relative frequency of GUVs populations with the lipid composition POPC/Cholesterol/PEG 2000-PE (75:20:5 molar ratio, 14 mM) fluorescently labeled with DOPE-NBD (0.7 mol%) and prepared in DexPEG hydrogel substrates with DS = 2 and PEG crosslinkers **1**, **2**, **4** and **5**.

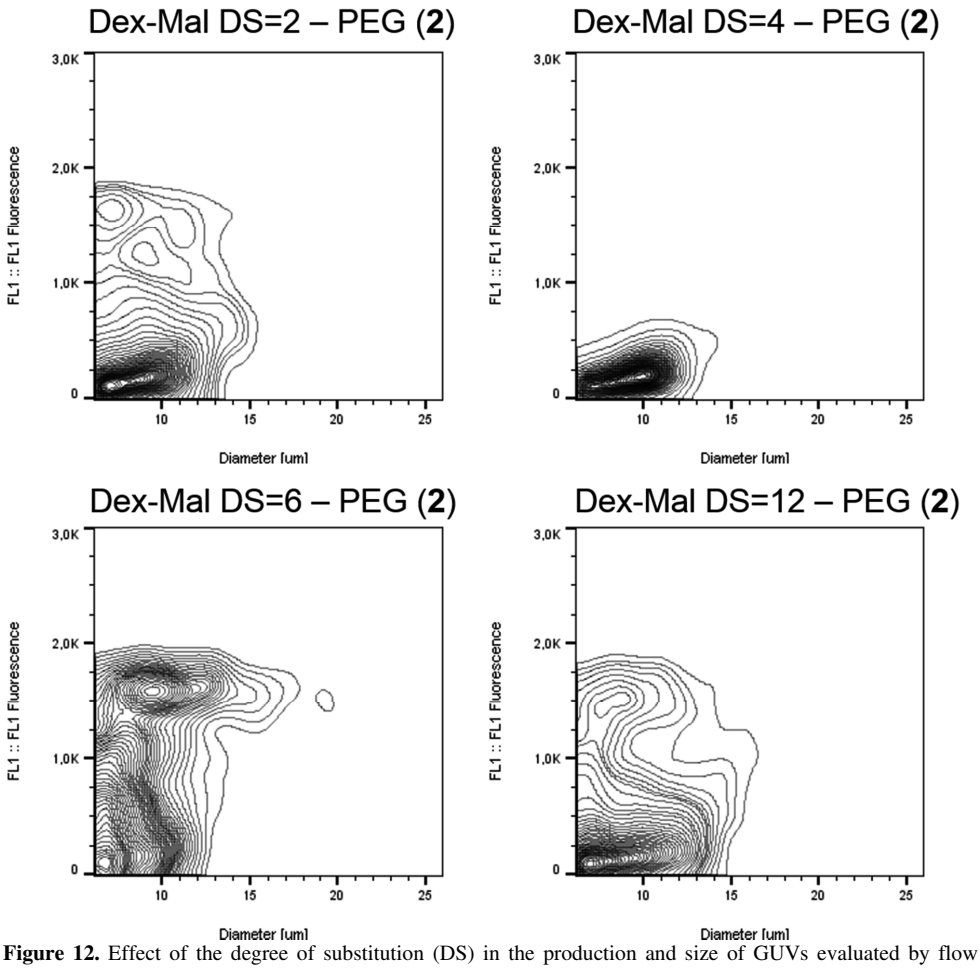

Figure 12. Effect of the degree of substitution (DS) in the production and size of GUVs evaluated by flow cytometry. Contour maps of the relative frequency of GUVs populations with the lipid composition POPC/Cholesterol/PEG 2000-PE (75:20:5 molar ratio, 14 mM) fluorescently labeled with DOPE-NBD (0.7 mol%) and prepared in DexPEG hydrogel substrates with DS = 2, 4, 6, 12 and PEG crosslinker **2**.

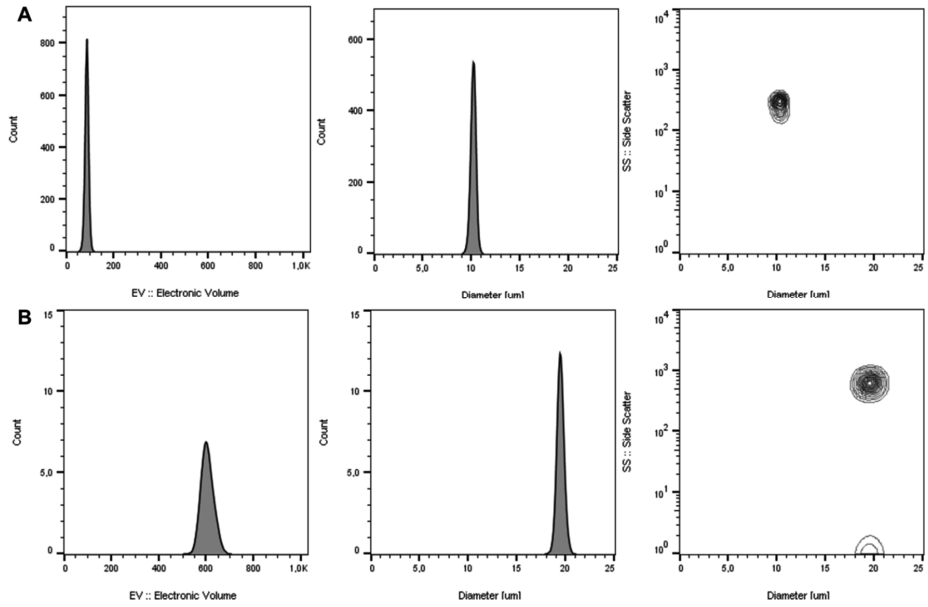

Figure 13. Verification of the diameter with NIST Traceable Latex Particles Standards. **A**) Histogram and contour map for latex particles with standard nominal of size 10 µm and **B**) Histogram and contour map for latex particle with standard nominal of size 20 µm.

Differential Scanning Calorimetry (DSC).

Temperature scans were performed in a Discovery DSC from TA instruments. The samples were scanned from -50 to 50 °C at a heating rate of 10 °C/min. The heat scans were performed and recorded two times. No difference was observed between the first and the second heating run. DSC traces for the first heating run are presented in **Figure 14**. The baseline was subtracted and the heat flow signal was normalized for all samples. A well-defined melting transition (T_m) was detected for pure DOPC lipid at -6 °C (black trace). This value is in good agreement with the value reported for hydrated DOPC (*ca* 3 H_2O).[36] Figure **Figure 14A** shows the DSC traces for both dry DexPEG hydrogel film (gray trace) and dry hybrid DOPC – DexPEG hydrogel film (blue trace). Thermal analysis indicates slight interaction between DOPC and DexPEG by the displacement of DOPC T_m to -12 °C and PEG T_m from 45 °C to 42 °C. In **Figure 14B** the strong interaction of DOPC lipid with PEG hydrogel is detected by 1 °C displacement of PEG T_m and the depression of the DOPC melting transition.

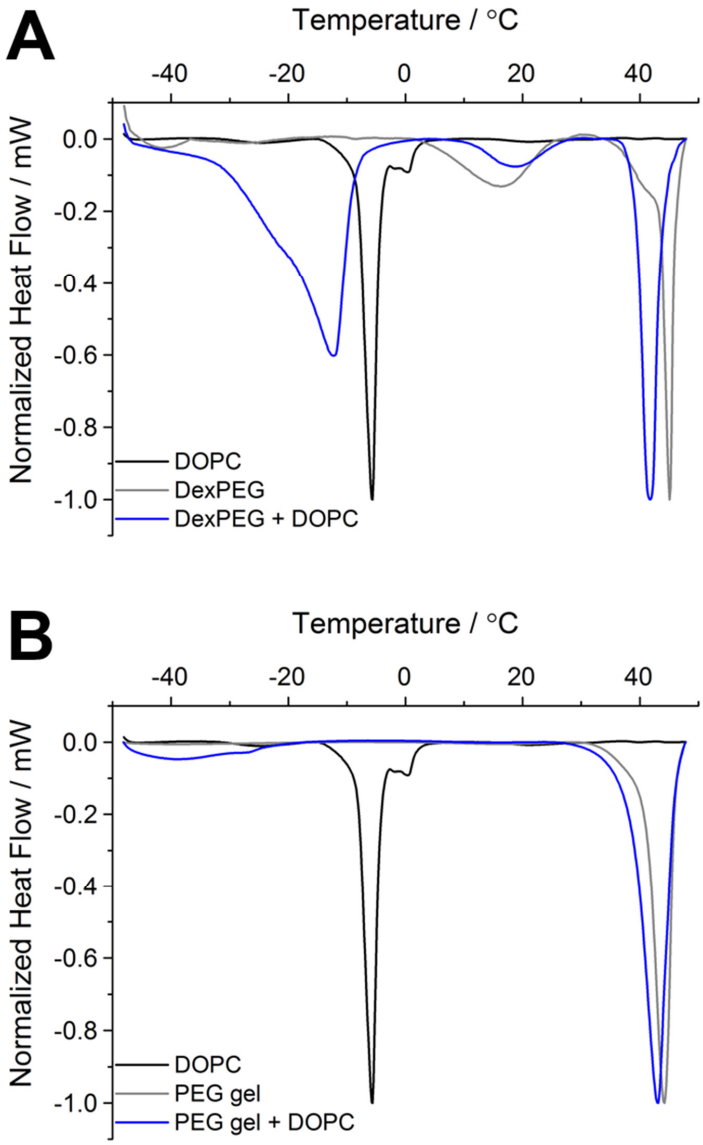

Figure 14. Thermal analysis of DexPEG and PEG hydrogels. **A**) Normalized Thermograms of DexPEG, DOPC and DexPEG - DOPC. **B**) Normalized Thermograms of PEG gel, DOPC and PEG gel - DOPC. The base line was subtracted for all the traces.

References

1. Fenz, S.F. & Sengupta, K. Giant vesicles as cell models. *Integr Biol-Uk* **4**, 982-995 (2012).
2. Tsai, F.C., Stuhrmann, B. & Koenderink, G.H. Encapsulation of Active Cytoskeletal Protein Networks in Cell-Sized Liposomes. *Langmuir* **27**, 10061-10071 (2011).
3. Menger, F.M. & Keiper, J.S. Chemistry and physics of plant vesicles as biomembrane models. *Curr Opin Chem Biol* **2**, 726-732 (1998).
4. Walde, P., Cosentino, K., Engel, H. & Stano, P. Giant Vesicles: Preparations and Applications. *Chembiochem* **11**, 848-865 (2010).
5. Lipowsky, R. The Morphology of Lipid-Membranes. *Curr Opin Struc Biol* **5**, 531-540 (1995).
6. Pautot, S., Frisken, B.J. & Weitz, D.A. Engineering asymmetric vesicles. *P Natl Acad Sci USA* **100**, 10718-10721 (2003).
7. Needham, D. & Evans, E. Structure and Mechanical-Properties of Giant Lipid (Dmpc) Vesicle Bilayers from 20-Degrees-C Below to 10-Degrees-C above the Liquid-Crystal Crystalline Phase-Transition at 24-Degrees-C. *Biochemistry-Us* **27**, 8261-8269 (1988).
8. Kato, A. et al. Phase Separation on a Phospholipid Membrane Inducing a Characteristic Localization of DNA Accompanied by Its Structural Transition. *J Phys Chem Lett* **1**, 3391-3395 (2010).
9. Hansen, J.S., Thompson, J.R., Helix-Nielsen, C. & Malmstadt, N. Lipid Directed Intrinsic Membrane Protein Segregation. *Journal of the American Chemical Society* **135**, 17294-17297 (2013).
10. Gutierrez, M.G. & Malmstadt, N. Human Serotonin Receptor 5-HT1A Preferentially Segregates to the Liquid Disordered Phase in Synthetic Lipid Bilayers. *Journal of the American Chemical Society* **136**, 13530-13533 (2014).
11. Horger, K.S. et al. Hydrogel-assisted functional reconstitution of human P-glycoprotein (ABCB1) in giant liposomes. *Bba-Biomembranes* **1848**, 643-653 (2015).
12. Motta, I. et al. Formation of Giant Unilamellar Proteo-Liposomes by Osmotic Shock. *Langmuir* **31**, 7091-7099 (2015).
13. Kahya, N. Protein-protein and protein-lipid interactions in domain-assembly: Lessons from giant unilamellar vesicles. *Bba-Biomembranes* **1798**, 1392-1398 (2010).
14. Koller, D. & Lohner, K. The role of spontaneous lipid curvature in the interaction of interfacially active peptides with membranes. *Bba-Biomembranes* **1838**, 2250-2259 (2014).
15. Tamba, Y. & Yamazaki, M. Magainin 2-Induced Pore Formation in the Lipid Membranes Depends on Its Concentration in the Membrane Interface. *J Phys Chem B* **113**, 4846-4852 (2009).
16. Tamba, Y., Ariyama, H., Levadny, V. & Yamazaki, M. Kinetic Pathway of Antimicrobial Peptide Magainin 2-Induced Pore Formation in Lipid Membranes. *J Phys Chem B* **114**, 12018-12026 (2010).
17. Akashi, K., Miyata, H., Itoh, H. & Kinosita, K. Preparation of giant liposomes in physiological conditions and their characterization under an optical microscope. *Biophysical Journal* **71**, 3242-3250 (1996).

18. Valkenier, H., Mora, N.L., Kros, A. & Davis, A.P. Visualization and Quantification of Transmembrane Ion Transport into Giant Unilamellar Vesicles. *Angew Chem Int Edit* **54**, 2137-2141 (2015).
19. Reeves, J.P. & Dowben, R.M. Formation and properties of thin-walled phospholipid vesicles. *Journal of Cellular Physiology* **73**, 49-60 (1969).
20. Angelova, M.I. & Dimitrov, D.S. Liposome Electroformation. *Faraday Discuss.* **81**, 303-+ (1986).
21. Chen, J., Park, H. & Park, K. Synthesis of superporous hydrogels: Hydrogels with fast swelling and superabsorbent properties. *J Biomed Mater Res* **44**, 53-62 (1999).
22. Shalaby, W.S.W., Blevins, W.E. & Park, K. Use of Ultrasound Imaging and Fluoroscopic Imaging to Study Gastric Retention of Enzyme-Digestible Hydrogels. *Biomaterials* **13**, 289-296 (1992).
23. Peppas, N.A., Hilt, J.Z., Khademhosseini, A. & Langer, R. Hydrogels in biology and medicine: From molecular principles to bionanotechnology. *Adv Mater* **18**, 1345-1360 (2006).
24. Henise, J., Hearn, B.R., Ashley, G.W. & Santi, D.V. Biodegradable Tetra-PEG Hydrogels as Carriers for a Releasable Drug Delivery System. *Bioconjugate Chem* **26**, 270-278 (2015).
25. Kim, T.G., Shin, H. & Lim, D.W. Biomimetic Scaffolds for Tissue Engineering. *Adv Funct Mater* **22**, 2446-2468 (2012).
26. Daniele, M.A., Adams, A.A., Naciri, J., North, S.H. & Ligler, F.S. Interpenetrating networks based on gelatin methacrylamide and PEG formed using concurrent thiol click chemistries for hydrogel tissue engineering scaffolds. *Biomaterials* **35**, 1845-1856 (2014).
27. Horger, K.S., Estes, D.J., Capone, R. & Mayer, M. Films of Agarose Enable Rapid Formation of Giant Liposomes in Solutions of Physiologic Ionic Strength. *Journal of the American Chemical Society* **131**, 1810-1819 (2009).
28. Lira, R.B., Dimova, R. & Rieke, K.A. Giant Unilamellar Vesicles Formed by Hybrid Films of Agarose and Lipids Display Altered Mechanical Properties. *Biophysical Journal* **107**, 1609-1619 (2014).
29. Weinberger, A. et al. Gel-Assisted Formation of Giant Unilamellar Vesicles. *Biophysical Journal* **105**, 154-164 (2013).
30. Garten, M. et al. Methyl-branched lipids promote the membrane adsorption of alpha-synuclein by enhancing shallow lipid-packing defects. *Phys Chem Chem Phys* **17**, 15589-15597 (2015).
31. Mora, N.L. et al. Preparation of size tunable giant vesicles from cross-linked dextran(ethylene glycol) hydrogels. *Chem Commun* **50**, 1953-1955 (2014).
32. Kim, S.H. & Chu, C.C. Synthesis and characterization of dextran-methacrylate hydrogels and structural study by SEM. *J Biomed Mater Res* **49**, 517-527 (2000).
33. Coulter, W.H. High speed automatic blood cell counter and cell analyzer. *Proc. Natl. Electron. Conf.*, 1034–1040 (1956).
34. Rodriguez-Trujillo, R. et al. Label-free protein detection using a microfluidic Coulter-counter device. *Sensor Actuat B-Chem* **190**, 922-927 (2014).
35. Shapiro, H.M. Practical Flow Cytometry. (Wiley, 2005).
36. Ulrich, A.S., Sami, M. & Watts, A. Hydration of Dopc Bilayers by Differential Scanning Calorimetry. *Bba-Biomembranes* **1191**, 225-230 (1994).

37. Moore, J.S. & Stupp, S.I. Room-Temperature Polyesterification. *Macromolecules* **23**, 65-70 (1990).
38. de Figueiredo, R.M., Oczipka, P., Frohlich, R. & Christmann, M. Synthesis of 4-maleimidobutyric acid and related maleimides. *Synthesis-Stuttgart*, 1316-1318 (2008).
39. R, C.W.H.a.H.W. *Google Patents* (1971).